RESEARCH ARTICLE

Simple solvothermal synthesis of a novel Er^{3+} and Nd^{3+} doped $Sr_2As_2O_7$ nanomaterials and investigation of catalytic performance for synthesis of organic compounds

Shahla Ekhtiyari [1], Leila Kafi-Ahmadi [1*], Shahin Khademinia [2]

[1] *Department of Inorganic Chemistry, Faculty of Chemistry, Urmia University, Urmia, Iran*

[2] *Department of Inorganic Chemistry, Faculty of Chemistry, Semnan University, Semnan 35351 19111, Iran*

ARTICLE INFO

Article History:
Received 2021-05-01
Accepted 2021-07-15
Published 2021-08-01

Keywords:
Solvothermal
nanocatalyst
Biginelli
Strontium Arsenate
Doping

ABSTRACT

Doping some lanthanide ions into $Sr_2As_2O_7$ crystal system is reported for the first time by a simple solvothermal method using $Sr(NO_3)_2$, As_2O_3, Er_2O_3 and Nd_2O_3 compounds. Characterization of the as-synthesized nanomaterials is done by powder X-ray (PXRD) analysis. Rietveld analysis data confirmed that the synthesized materials were crystallized in a mixture of three crystal phases. FESEM images revealed that dopant ion type had a considerable effect on the morphology of the final product. The data showed that the morphology of the synthesized materials were comb-like structure and particle. Direct band gap energy (Eg) of the materials obtained using ultraviolet-visible spectra showed that the Eg was about 3.5 eV. The synthesized nanomaterials were used as catalyst in the Biginelli reactions. The data confirmed that the materials could behave as Lewis acid catalyst in the reactions. The catalytic performance of the synthesized sample was 92% when the catalyst amount was 0.03 g, reaction temperature was 90 °C and the reaction time was 100 min.

How to cite this article
Ekhtiyari Sh., Kafi-Ahmadi L., Khademinia Sh. Simple solvothermal synthesis of a novel Er^{3+} and Nd^{3+} doped Sr2As2O7 nanomaterials and investigation of catalytic performance for synthesis of organic compounds. J. Nanoanalysis., 2021; 8(3): 233-242. DOI: 10.22034/jna.008.

INTRODUCTION

Among $A^{II}As^{V}O$ materials (A is the alkaline earth element), $Sr_2As_2O_7$ has been studied more in several works [1-3]. It had been reported that $Sr_2As_2O_7$ is crystallized in tetragonal crystal system with the space group $P4_3$ and $P4_1$ [4]. However, we have recently reported a new monoclinic crystal system with the space group of $P2_1$ and the lattice parameters of a=5.34918 Å, b=11.32062 Å and c=8.20518 Å with β=91.313 ° [5]. $Sr_2As_2O_7$ has been synthesized previously by solid state [6-8] and hydrothermal [5] methods. The advantages of the hydrothermal method compared to solid state methods are the lower reaction temperature (180 °C), mild reaction condition and nano sized obtained materials. The obvious difference in the obtained crystal system type by changing the reaction method can be due to the different reaction conditions including time, temperature, pressure, solvent and raw material type. Until now, there is no report in the literature about doping the metal ions into $Sr_2As_2O_7$ crystal structure. The Biginelli reaction is a method for the synthesis of DHPMs in one-step process. Several metal oxides as nanocatalysts have been used in Biginelli reactions summarized in ref. [9-15]. Recently, we have reported the catalytic performance of pure $Sr_2As_2O_7$ nanomaterial for the synthesis of DHPMs compounds by Biginelli reactions [16].

The present research work reports the solvothermal synthesis of Er^{3+} and Nd^{3+} doped $Sr_2As_2O_7$. PXRD patterns are studied by Rietveld analysis using *FullProf* software. As per our knowledge, there is no report about the synthesis and catalytic application of the doped $Sr_2As_2O_7$

* Corresponding Author Email: *l.kafiahmadi@urmia.ac.ir*

This work is licensed under the Creative Commons Attribution 4.0 International License.
To view a copy of this license, visit http://creativecommons.org/licenses/by/4.0/.

nanomaterials. The physical properties of the as-synthesized nanomaterials are investigated by FESEM, UV-Vis and FTIR spectroscopies. The catalytic performance of the as-synthesized nanomaterials is studied in Biginelli reactions. The comparison between the catalytic activities of the two synthesized samples is also studied.

EXPERIMENTAL

Materials and instruments

All chemicals including As_2O_3, $Sr(NO_3)_2$, Er_2O_3, Nd_2O_3, C_2H_5OH and KOH were of analytical grade, obtained from commercial source (Merck Company) and used without further purifications. Absolute C_2H_5OH was used. The purity of the other materials was 99%. Phase identifications were performed on an X-ray powder diffractometer D5000 (Siemens AG, Munich, Germany) using CuK_α radiation. The XRD apparatus used for the crystallographic study had monochromator. *FullProf* software was used to perform Rietveld analysis. Several crystallographic data including lattice parameter, residual factor (R_F), Bragg residual factor (R_{Bragg}), goodness of refinement (χ^2), crystal phase type and purity values were obtained by the analysis. Hitachi FE-SEM model S-4160 was used to study the morphology of the obtained materials. UV-visible spectrophotometer model-UV-1650 PC (Shimadzu, Japan) was used to record the absorption spectra. Tensor 27 spectrometer (Bruker Corporation, Germany) was used to take FTIR spectra. The purity of the Biginelli reaction products was checked by thin layer chromatography (TLC) on glass plates coated with silica gel 60 F254 using n-hexane/ethyl acetate mixture as mobile phase. Thermo scientific 9100 apparatus was used to record the melting points of the DHPMs compounds.

Solvothermal synthesis of Er^{3+} and Nd^{3+} doped $Sr_2As_2O_7$

Er and Nd-doped $Sr_2As_2O_7$ are synthesized by following process: 0.212 g (1.0 mmol) of $Sr(NO_3)_2.5H_2O$ (Mw = 211.62 g mol^{-1}), 0.198 g (1.0 mmol) of As_2O_3 (Mw = 197.87 g mol^{-1}) and 0.025 mmol of Er_2O_3 (S_1) or Nd_2O_3 (S_2) were added to 10 mL of distilled water. Then, 20 mL of ethanol was added to the resultant mixture. The pH value of the solution is 5. The solution was stirred for 15 min at 60 °C. Certain volume of 4M KOH was added to the solution while stirring until the pH value was reached to 12. The resultant solution was stirred more for 15 min and then ultrasonicated for 30 min at room temperature. After transferring the solution into a 60-mL Teflon lined stainless steel autoclave, it was sealed and heated at 200 °C for 24 h. The autoclave was cooled immediately by water to room temperature when the certain reaction time was finished. A white - colored powder was obtained, washed with distilled water and dried at 120 °C for 20 min under normal atmospheric condition.

General procedure to synthesize of DHPMs

In a typical procedure, a mixture of benzaldehyde, ethyl acetoacetate, and urea with the molar ratio of 1:1:1.2, respectively, and a certain amount of catalyst ($Sr_2As_2O_7$) were poured into a round bottom flask. The suspension was stirred at desired reaction temperature which was designed by the design expert software. At the certain designed time, the solid product was separated and washed by distilled water to separate the unreacted raw materials. Then, the obtained crude DHPM was dissolved in ethanol to separate $Sr_2As_2O_7$ and crystallized at room temperature to obtain the pure DHPM. The experimental designed procedure summarized in Table 3 was performed by changing the reaction parameters simultaneously. The reaction yield for each designed test was calculated by measuring the mmole fraction of the final product.

RESULTS AND DISCUSSIONS

Characterization

XRD analysis

The X-ray diffraction patterns of the as-synthesized doped $Sr_2As_2O_7$ samples are reported in Fig. 1 a-e. Structural analysis was performed by *FullProf* program, employing profile matching with constant scale factor. Fig. 1 a and b indicates that the patterns have a main $Sr_2As_2O_7$ monoclinic crystal system with space group $P2_1$ for S_1 [16]. However, the refinement of the patterns showed that impure crystal phases are found in the composites. $Sr_2As_2O_7$ (60%), $SrCO_3$ (28%) and As_2O_3 (12%) crystal phases were found when Nd^{3+} is doped into the crystal system. Besides, the data show that when Er^{3+} is introduced in the crystal system, the mixture is composed of $Sr_2As_2O_7$ (91%), $SrCO_3$ (4%) and As_2O_3 (5%).

The data included in Tables 1 and 2 present some of the crystallographic parameters of the as-prepared nanomaterials. The unit cell volume data

CC BY

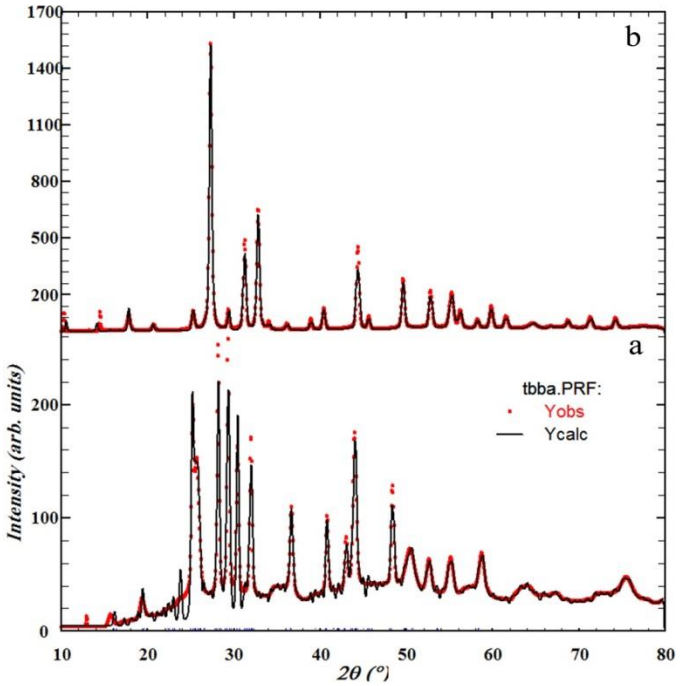

Fig. 1. XRPD patterns of a) S_1 and b) S_2.

Table 1. Cell parameters, cell volume, β and interplanar spacing data of the as-prepared nanocomposites.

Compound	a (Å)	b (Å)	c (Å)	V (Å³)	β°	d (A˚)
S_1	5.32471	11.34114	8.11172	489	91.29581	3.071
S_2	5.31820	10.98942	8.14083	475	91.29276	3.069

Table 2. Rietveld analysis data, Counts, purity, crystallite size and dislocation density data of the as-prepared nanocomposites.

Compound	R_{Bragg}	R_F	χ^2	Intensity (monoclinic Structure)	purity	D	δ
S_1	1.99	0.92	1.34	274	60	24	17.3
S_2	3.84	2.47	2.45	1536	91	24	17.3

show that the parameter value is decreased when Er^{3+} is doped into the crystal system. This can be due to the smaller ionic radii of Er^{3+} compared to Nd^{3+}. As could be found from Table 2, it is clear that the count value representing the crystal phase growth of the materials is decreased when Er^{3+} is doped into the crystal system. The value of the dislocation density δ [(lines/m²)10^{14}], which is related to the number of defects in the crystal was calculated from the average values of the crystallite size (D) by the relationship given by $\delta = \frac{1}{D^2}(2)$ equation reveal that there is no observable dislocation density change due to changing the dopant ions type into the crystal system.

Morphology analysis

Fig. 2 a and b introduces the FESEM images of S_1 and S_2, respectively. The images show that the morphology the material was comb-like structure when Nd^{3+} is doped into the crystal system. However, when Er^{3+} is doped, the morphology is particle. The data presented in Fig. 2 c and d show the particle size distribution profiles of S_1 and S_2, respectively. The data reveal that the thickness size of the comb-like structure are in 80-100 nm range. However, it was found that the most abundance of the diameter size of the synthesized particles is more than 100 nm for S_2.

Elemental analysis

Fig. 3 a - b illustrates the EDX analyses for the samples doped theoretically with 0.05 mmol of the lanthanide dopants ions into the crystal system which verify the doping and the compositional

(cc) BY

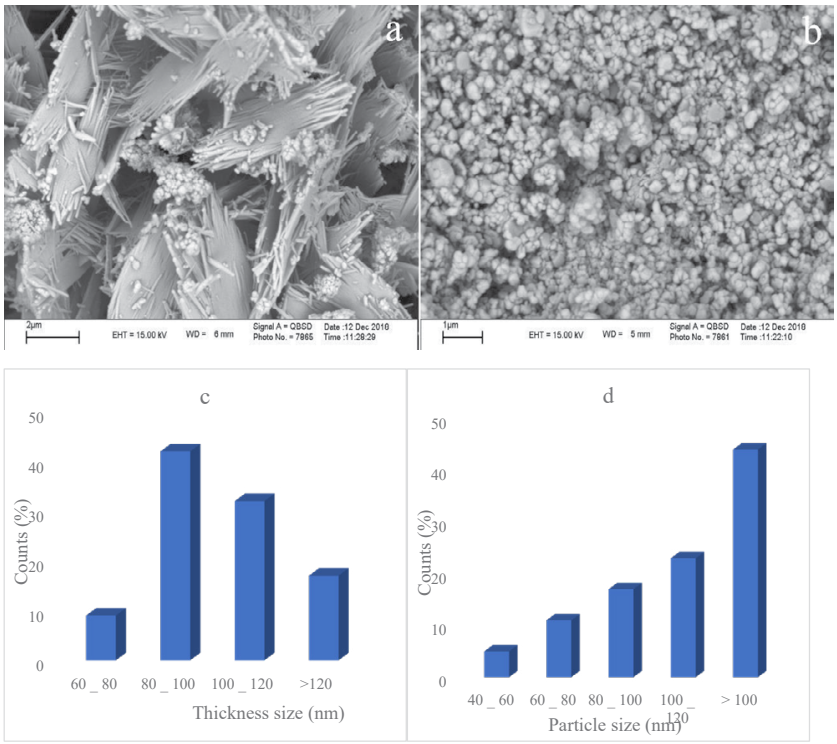

Fig. 2. FESEM images of a) S_1 and b) S_2 and particle size distribution profile of c) S_1 and d) S_2.

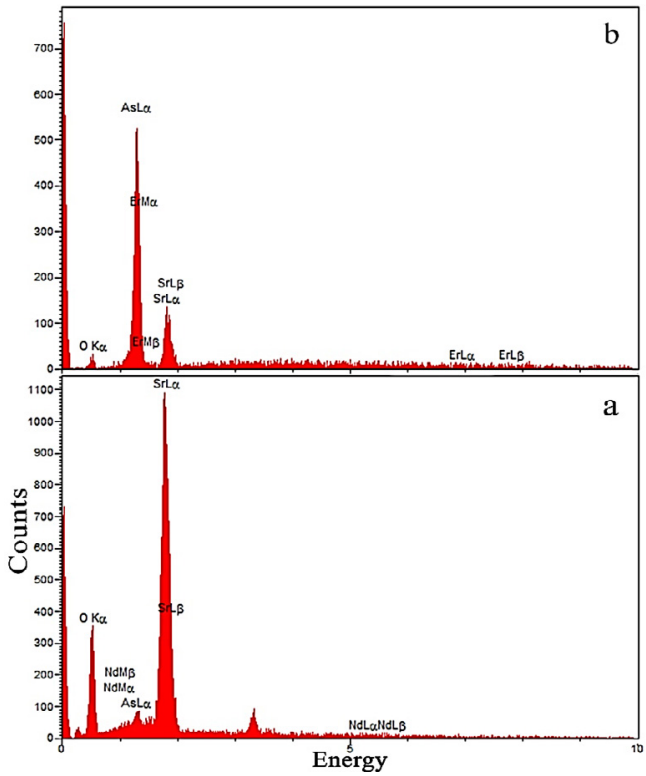

Fig. 3. EDX spectra of a) S_1 and b) S_2.

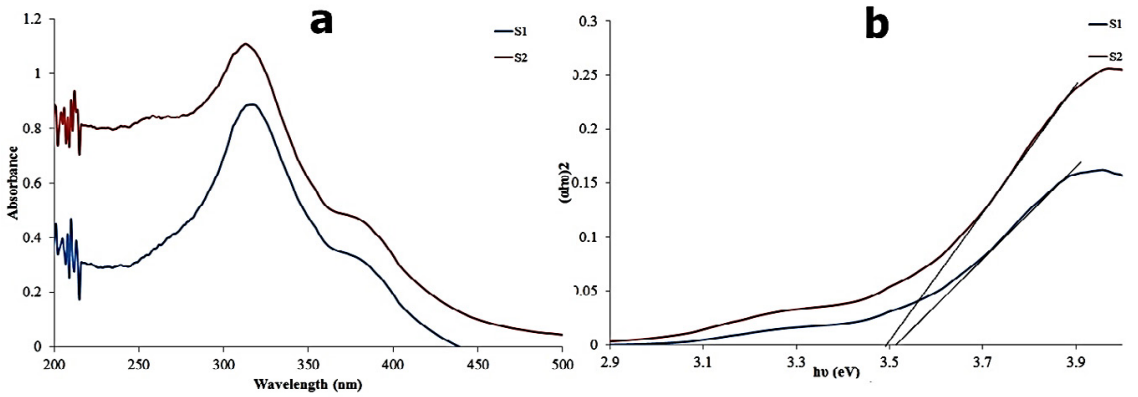

Fig. 3. Plots of a) UV-Vis and b) direct band gap energies of the as-prepared nanocomposites.

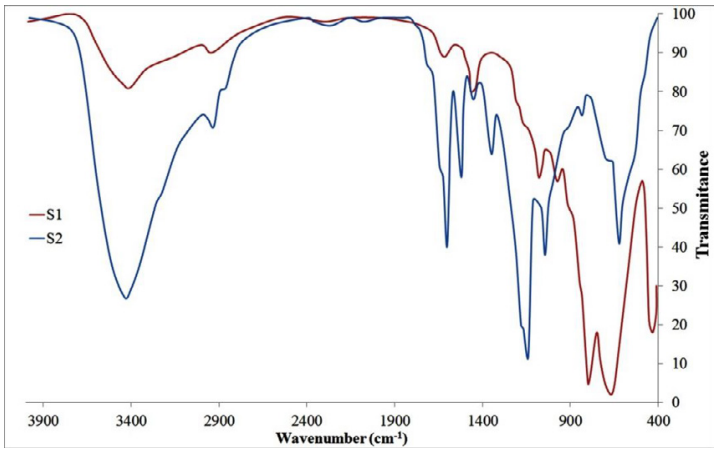

Fig. 4. FTIR spectra of the as-fabricated nanocomposites.

analysis of Nd^{3+} or Er^{3+} in the composite. The peaks corresponded to Nd or Er and (Sr, As and O) atoms present in the samples are labeled. The respective energy positions and the specific X-ray lines from various elements are also indicated. The A% values of the dopants in the obtained samples and investigating the capacity of the sample to accept the ions in the crystal systems is reported. The A% values are 0.021 and 0.032 for Nd and Er, respectively, doped nanomaterials. However, it is clear that the decrease is not considerable, the data reveal that when a lighter ion is included in the crystal system, the capacity of the crystal system to accept the ion is decreased. According to the literature, the ionic radii (Coordination number) of Sr^{2+} (VI) = 1.18, As^{5+} (VI) = 0.58, Nd^{3+} (VI) = 0.98, Er^{3+} (VI): 0.89 Å [17].

The difference between the intensity of the peaks in Fig. 3 a is attributed to Sr and As may be due to the higher amount and heaver atomic weight of Sr to As in the mixture that is confirmed by the map images found in the supplementary information.

Optical Property

UV-Vis absorption spectra of the as-synthesized samples are shown in Fig. 4a. The direct optical band gap energy is also shown in Fig. 4b. The absorption data indicate that the as-synthesized nanocomposites possess a typical visible absorption edge at about 350 nm. The relation between the absorption coefficient and incident photon energy can be written as $(\alpha h\nu)^2 = A(h\nu - Eg)$ for direct band gap energy. In this equation, A and Eg are constant value and direct band gap energy, respectively [31]. To measure the direct band gap energy, the linear part of the curve to the energy axis was extrapolated. Fig. 5 b indicates that the synthesized materials show a strong band structure at 3.5 eV.

Fig. 4 presents the FTIR spectra of the obtained samples. The peaks at about 430, 650, 800, 850,

(cc) BY

1030, 1150, 1500, 1600 and 3400 cm^{-1} are observed in the spectra. The figure shows an important point. It is found that the more intensity of the peaks of a spectrum the more purity of the material. The discussion found in the characterization section indicates that the purity of S_2 is much more than S_1. The strong band at 430 cm^{-1} is assigned to the As–$O_{bridging}$ stretching vibration [18]. The absorption at 650 cm^{-1} is assigned to Sr–O stretching vibration [19]. The bands at 800 and 1030 cm^{-1} are related to As–O vibration modes [20]. The band at 800 cm^{-1} is assigned to stretching vibrations of As–O bonds [21,22]. The peaks at 1500 and 3400 cm^{-1} are related to the H-O vibration modes of free H_2O [23].

Biginelli catalytic process

Achieving optimal conditions by response surface methodology

Full factorial design is a design combining all possible combination of affecting factors on the reaction yield and their settings. Three levels of the factor setting is usual in chemical reaction that can be due to the determination of all main effects and all interaction effects of the involved factors (catalyst, time, temperature in the present work) with small number of experiments (Table 3). There is a method in the literature naming response surface methodology (RSM) that analyzes the experimental design by mathematical and statistical method by applying an empirical model. To evaluate the model, analysis of variance (ANOVA) was used (Table 4). A proper analysis of variance requires some replicate experiments. In the present Biginelli reaction study, determination the amount of nanocatalyst, time and temperature in which the reaction is performed completely, is investigated. The response is the obtained yield (%). Equation 1 presents the relation between the factors and the yield of the Biginelli reaction, Y%, based on the first order model:

$$Y\% = -87.14746 + 5.18178 \times Catalyst + 1.24024 \times time + 0.19943 \times temperature - 0.027500 \times Catalyst \times time - 0.037460 \times Catalyst^2 \quad (1)$$

The data included in Table 4 and the coefficient in the equation indicate that the more the value is, the more the effect is. It is clear that the effect of catalyst is higher than the effect of the others, moreover, the

Table 3. Three-level full factorial design in Biginelli reaction*.

Catalyst (mg)	Time (min)	Temperature (°C)	Yield %
40	100	40	86
20	100	40	79
40	50	90	79
30	75	65	83
30	75	65	79
20	50	40	40
40	100	90	89
30	75	65	80
20	50	90	50
20	100	90	85
30	75	65	82
40	50	40	77
30	75	107	94
30	117	65	94
30	33	65	65
46	75	65	83
13	75	65	58
30	75	65	71
30	75	23	66
30	75	65	81

* Benzaldehyde: Ethyl acetoacetate: Urea molar ratios is as follows: 1:1:1.2.

CC BY

Table 4. Analysis of variance for suggested first-order model.

Source	Sum of Squares	df	Mean Square	F Value	p-value Prob > F	
Block	2.7	1	2.7			
Model	3432.851	5	686.5701	29.03522	< 0.0001	significant
A-Catalyst	1037.696	1	1037.696	43.88444	< 0.0001	
B-time	1471.737	1	1471.737	62.24013	< 0.0001	
C-temperature	339.4834	1	339.4834	14.35684	0.0023	
AB	378.125	1	378.125	15.991	0.0015	
A^2	205.8087	1	205.8087	8.7037	0.0113	
Residual	307.3995	13	23.64611			
Lack of Fit	247.3995	9	27.48883	1.832589	0.2930	not significant
Pure Error	60	4	15			
Cor. Total	3742.95	19				

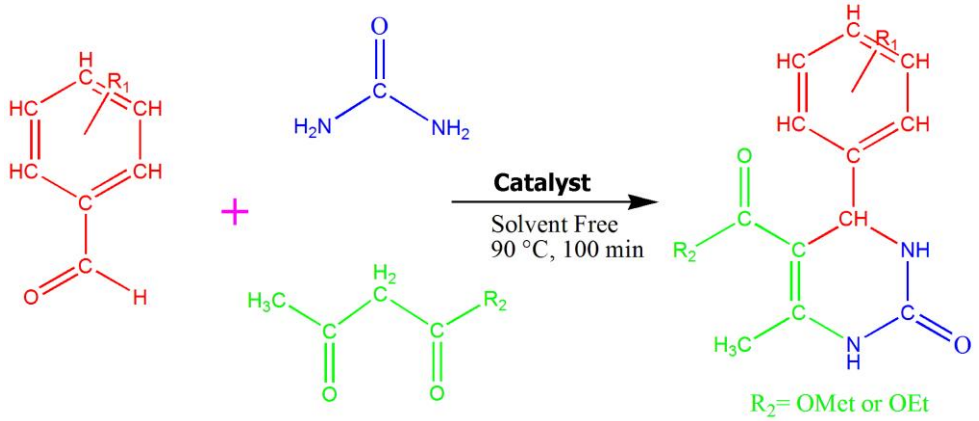

Scheme 1. Typical Biginelli reaction process using the synthesized nanomaterials as catalyst.

effect of the time and temperature are close to each other.

Scheme 1 shows a summary of the present Biginelli reaction pathway. As we could find from the optimization results obtained by design expert software, it was revealed that 60 mg of the catalyst, 90 °C reaction temperature, and 100 min reaction time were the optimum parameters for the synthesis of DHPMs. The optimized parameters were used for the synthesis of other DHPM derivatives.

The response surface methodology (RSM) was used to investigate the influence of the three factors (catalyst, time, temperature) on the present Biginelli reaction. Fig. ***5*** represents the 2D and 3D plots related to the interaction of AB. The curvature of the plots indicates the interaction between the variables. In other words, by increasing the reaction temperature at a constant reaction time (AB interaction), high surface area of catalyst is available for the raw materials molecules leading to enhance the DHPM derivatives production percentage.

Table 5 presents the catalytic activity data of pure $Sr_2As_2O_7$ nanomaterial at the optimized conditions using different raw materials derivatives. The purity of the as-prepared DHPMs compounds is checked by measuring the melting points of the recrystallized DHPMs. The data show that the most reaction yield is obtained when 3-NO_2 is used as benzaldehyde derivatives. However, when 2-OMet is used, the least reaction yield was achieved. The observation reveals that when the substitution group on the benzaldehyde ring is on meta position, the reaction yield is high that can be due to the higher election affinity effect on the position. However, when the methoxy group is on

(cc) BY

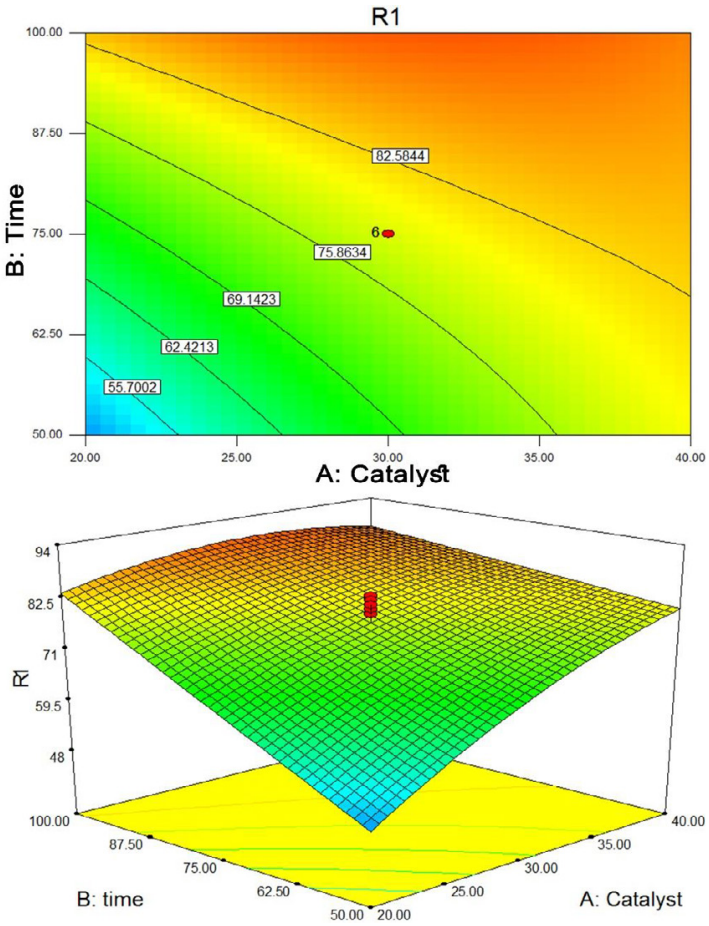

Fig. 5. 2D and 3D plots related to the interaction of AB for the pure $Sr_2As_2O_7$ nanomaterial.

Table 5. Efficiency of pure $Sr_2As_2O_7$ for the synthesis of the DHPMs compounds.

R_1	R_2	R%	Melting Point (°C)	
			Reported	Measured
H	OEt	92	197-201	198-200
4-Cl	OEt	87	208-210	209-211
2-Cl	OEt	85	214-219	215-217
4-Br	OEt	81	211-213	213-214
3-NO_2	OEt	95	224-225	225-226
2-OMe	OEt	75	261-263	262-263
3-OMe	OEt	46	256-258	258-259
3-OH	OEt	59	165-167	164-165
4-OH	OEt	66	252-255	255-257
H	OMe	88	203-206	206-207
4-Cl	OMe	84	201-205	204-207
2-Cl	OMe	90	226-228	228-229
4-Br	OMe	61	238-241	242-244
3-NO_2	OMe	93	277-280	279-280
2-OMe	OMe	27	282-286	283-285
3-OMe	OMe	57	191-197	192-195
4-OH	OMe	36	238-243	241-242

Table 6. A comparison study between the efficiency of the as-synthesized nanomaterials for the synthesis of the DHPMs compounds.

R	Yield (%)	
	S_1	S_2
H	89	86
4-Cl	67	59
2-Cl	83	77
3-OMe	51	43
3-OH	74	68
3-NO_2	85	80

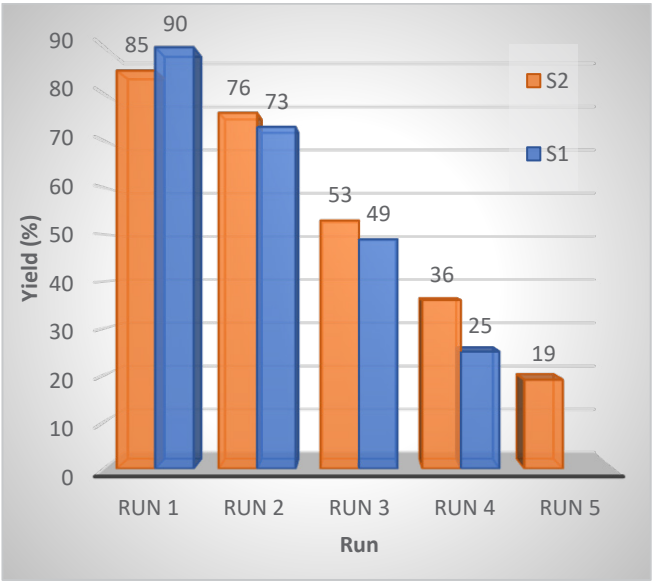

Fig. 6. Reusability comparison between S_1 and S_2 for the synthesis of DHPMs compounds.

ortho position, the electron affinity is weak and so the reaction cannot start efficiently.

A comparative study on the catalytic efficiency (Y%) of S_1 and S_2 is presented in Table 6. The data included in the table reveal that the efficiency of S_1 is more than S_2 at the same reaction conditions. However, the difference between the yield for S_1 and S_2 is not considerable. The data reveal that the more electron affinity of the substitution group, the more reaction yield.

Fig. 6 presents the reusability of the synthesized nanomaterials for the synthesis of the DHPMs compounds. The data reveals that the materials are stable considerably until run 3 in the synthesis process. Besides, it is found that S_1 is more stable during the synthesis process that can be due to the larger particle size distribution.

CONCLUSION

The aim and purpose of the present work was reporting a study on the synthesis of Nd^{3+} and Er^{3+} doped $Sr_2As_2O_7$ nanomaterials and using the materials as high efficient and recyclable catalysts for the synthesis of DHPMs. A green synthesis was used for the synthesis of the materials. The rietveld analysis data revealed that a three component crystal phases as composite were obtained when the dopant ions were included in the system. FESEM images showed that the morphology of the obtained materials was changed from comb structure to homogeneous particles when the dopant type was changed. When the nanomaterials were used as nanocatalyst, it was found that the optimum conditions for the synthesis of DHPMs compounds were 30 mg of catalyst, 100 °C reaction temperature and 90 min reaction time.

(cc) BY

CONFLICT OF INTEREST

The authors declare that there is no conflict of interests regarding the publication of this manuscript.

REFERENCE

1. Weil M. Cadmium(II) diarsenate(V), Cd2As2O7. Acta Crystallographica Section E Structure Reports Online. 2001;57(4):i28-i9.
2. Harvey CF, Ashfaque KN, Yu W, Badruzzaman ABM, Ali MA, Oates PM, et al. Groundwater dynamics and arsenic contamination in Bangladesh. Chemical Geology. 2006;228(1-3):112-36.
3. Raičević S, Stanić V, Kaludjerović-Radoičić T. Theoretical Assessment of Calcium Arsenates Stability: Application in the Treatment of Arsenic Contaminated Waste. Materials Science Forum. 2007;555:131-6.
4. Weil M, Kolitsch U. Crystal structures of the triclinic low-temperature modifications of $Co_2As_2O_7$ and $Ni_2As_2O_7$. Poster, Annual Meeting of the DGK, Köln, Germany, February 28 - March 4, Abstract in Zeitschrift für Kristallographie., Suppl. 2005; No. 22: 183.
5. Khademinia S, Behzad M, Kafi-Ahmadi L, Hadilou S. Solar Light Photocatalytic Degradation of Malachite Green by Hydrothermally Synthesized Strontium Arsenate Nanomaterial through Response Surface Methodology. Zeitschrift für anorganische und allgemeine Chemie. 2018;644(4):221-7.
6. Weil M, Đorđević T, Lengauer CL, Kolitsch U. Investigations in the systems Sr–As–O–X (X=H, Cl): Preparation and crystal structure refinements of the anhydrous arsenates(V) Sr3(AsO4)2, Sr2As2O7, α- and β-SrAs2O6, and of the apatite-type phases Sr5(AsO4)3OH and Sr5(AsO4)3Cl. Solid State Sciences. 2009;11(12):2111-7.
7. Mbarek A, Edhokkar F. The $P4_3$ enantiomorph of $Sr_2As_2O_7$. Acta Cryst. E. 2013; 69: 84-86.
8. Gmelins Handbuch der Anorganischen Chemie 29 Strontium. Supplement, eighth ed. Verlag Chemie, Weinheim, Germany, 1960, p. 290.
9. Khademinia S, Behzad M, Alemi A, Dolatyari M, Sajjadi SM. Catalytic performance of bismuth pyromanganate nanocatalyst for Biginelli reactions. RSC Advances. 2015;5(87):71109-14.
10. Siddiqui ZN. Bis[(L)prolinato-N,O]Zn–water: A green catalytic system for the synthesis of 3,4-dihydropyrimidin-2 (1H)-ones via the Biginelli reaction. Comptes Rendus Chimie. 2013;16(2):183-8.
11. Sheykhan M, Yahyazadeh A, Ramezani L. A novel cooperative Lewis acid/Brønsted base catalyst Fe 3 O 4 @SiO 2 -APTMS-Fe(OH) 2 : An efficient catalyst for the Biginelli reaction. Molecular Catalysis. 2017;435:166-73.
12. Barthelemy A-L, Magnier E. Recent trends in perfluorinated sulfoximines. Comptes Rendus Chimie. 2018;21(8):711-22.
13. Kolvari E, Koukabi N, Hosseini MM. Perlite: A cheap natural support for immobilization of sulfonic acid as a heterogeneous solid acid catalyst for the heterocyclic multicomponent reaction. Journal of Molecular Catalysis A: Chemical. 2015;397:68-75.
14. Sanchez LM, Sathicq ÁG, Romanelli GP, González LM, Villa AL. Activity of immobilized metallic phthalocyanines in the multicomponent synthesis of dihydropyridine derivatives and their subsequent aromatization. Molecular Catalysis. 2017;435:1-12.
15. Khademinia S, Behzad M. Catalytic performance of bismuth pyromanganate nanocatalyst for Biginelli reactions. RSC Advances. 2015; **5:** 24313-24318.
16. Esmaeili R, Kafi-Ahmadi L, Khademinia S. A highly efficient one-pot multicomponent synthesis of 3,4-dihydropyrimidin-2-(1H)-ones/thiones catalyzed by strontium pyroarsenate nano-plates. Journal of Molecular Structure. 2020;1216:128124.
17. David R. Lide, ed., CRC Handbook of Chemistry and Physics, Internet Version 2006, Taylor and Francis, Boca Raton, FL, 2006; 1803-1804.
18. Weil M, Đorđević T, Lengauer CL, Kolitsch U. Investigations in the systems Sr–As–O–X (X=H, Cl): Preparation and crystal structure refinements of the anhydrous arsenates(V) Sr3(AsO4)2, Sr2As2O7, α- and β-SrAs2O6, and of the apatite-type phases Sr5(AsO4)3OH and Sr5(AsO4)3Cl. Solid State Sciences. 2009;11(12):2111-7.
19. Greena JAM, Karuppasamy K, Antony R, Shajan XS, Kumaresan S. Effect of Magnesium Doping on the Physicochemical Properties of Strontium Formate Dihydrate Crystals. Chemical Science Transactions. 2012;2(1):141-6.
20. Gmelins Handbuch der Anorganischen Chemie 29 Strontium. Supplement, eighth ed. Verlag Chemie, Weinheim, Germany, 1960, p. 290.
21. Bishay A, Maghrabi C. Properties of Bismuth Glasses in Relation to Structure. Physics and Chemistry of Glasses. 1969; 10: 1-11.
22. Srinivasarao G, Veeraiah N. Study on various physical properties of PbO–As2O3 glasses containing manganese ions. Journal of Alloys and Compounds. 2001;327(1-2):52-65.
23. Khademinia S, Behzad M. Low temperature hydrothermal synthesis, characterization and optical properties of strontium pyroniobate. Advanced Powder Technology. 2015;26(2):644-9.

CC BY